Letter

Isotropic single-gap superconductivity of elemental Pb

Rustem Khasanov,[1,*] Debarchan Das,[1] Dariusz Jakub Gawryluk,[2] Ritu Gupta,[1] and Charles Mielke III[1]
[1]*Laboratory for Muon Spin Spectroscopy, Paul Scherrer Institut, CH-5232 Villigen PSI, Switzerland*
[2]*Laboratory for Multiscale Materials Experiments, Paul Scherrer Institut, Villigen CH-5232, Switzerland*

(Received 21 June 2021; revised 20 August 2021; accepted 20 September 2021; published 29 September 2021)

The unconventional multigap superconductivity in elemental Pb were reported previously by the surface sensitive tunneling experiments as well as predicted by several theory works. To obtain bulk evidence for such multiple gap behavior, the thermodynamic critical-field B_c was measured along three different crystallographic directions ([100], [110], and [111]) in a high-quality Pb single crystal by means of muon spin rotation/relaxation. No difference in temperature evolution of B_c for all three directions was detected. The average reduced gap $\alpha = \Delta/k_B T_c = 2.312(3)$ (Δ is the zero-temperature gap value, and T_c is the transition temperature) was further obtained by employing the phenomenological α model. Our results imply that the elemental Pb is an *isotropic* superconductor with a *single* energy gap.

DOI: 10.1103/PhysRevB.104.L100508

Superconductivity was first discovered by Kamerlingh Onnes in elemental Hg in 1911 [1], and then in elemental Sn and Pb within the next 2 yr [2]. To date, 31 elements are known to be superconducting at ambient pressure [3] and, among them, Pb has the second highest superconducting transition temperature $T_c \simeq 7.20$ K, just after elemental Nb with $T_c \simeq 9.2$ K.

The description of lead within the weak-coupled BCS formalism was unsuccessful, thus, leading to the corresponding development of the strong-coupled extension within the framework of the Eliashberg theory (see Ref. [4] and references therein). The "unconventional" aspects of superconductivity in Pb in relation to the "conventional" BCS ones were discussed in a series of papers [4–14]. In particular, the presence of, at least, two separate superconducting energy gaps with distinct values were reported experimentally [10–12] as well as proposed theoretically [13,14].

Evidence for multigap superconductivity should be present in the temperature evolution of various thermodynamic quantities, e.g., electronic specific heat, entropy, critical fields, etc. Among them, the thermodynamic critical field B_c, which is related to the condensation energy of superconducting carriers via [15]:

$$\frac{B_c^2(0)}{4\pi} = N_F(0)\Delta^2 \tag{1}$$

[$B_c(0) = B_c(T = 0)$, $N_F(0)$ is the density of states at the Fermi level, and Δ is the zero-temperature value of the superconducting energy gap], becomes a direct probe of multiple superconducting energy gaps [16–19], as well as allows one to probe the superconducting gap anisotropy [20–22]. As the temperature dependence of B_c normalized to its zero-temperature value follows very closely a nearly quadratic behavior, the deviation function $D(T)$ is normally considered:

$$D(T) = \frac{B_c(T)}{B_c(0)} - \left[1 - \left(\frac{T}{T_c}\right)^2\right]. \tag{2}$$

By combining experimental data of Refs. [10–12], the "big" and the "small" reduced gaps in Pb were found to stay in the range of $\alpha_{big} = \Delta_{big}/k_B T_c = 2.21$–$2.31$ and $\alpha_{small} = \Delta_{small}/k_B T_c = 1.87$–$2.07$. The corresponding deviation functions, calculated by employing the α model of Padamsee *et al.* [23] and Johnston [24]), are shown in Fig. 1. It should be stressed, however, that experiments pointing to the presence of two distinct superconducting energy gaps in elemental Pb have been performed so far by means of tunneling only, i.e., by a surface sensitive technique. It is not obvious if the "intrinsic" gap functions measured in the bulk would remain the same as at the surface. Note that disagreement between theory and tunneling data have already been mentioned by Saunderson *et al.* in Ref. [14].

In this Letter, in order to test whether the superconducting gap structure of elemental lead is of a single- or a two-gap type, measurements of the thermodynamic critical-field $B_c(T)$ along three crystallographic directions were performed by means of the muon-spin rotation/relaxation (μSR) technique. Experiments were carried out by applying the external magnetic-field B_{ex} along [100], [110], and [111] axes. The selection of these orientations comes from the face-centered cubic crystal structure of Pb where the strongest differences in physical quantities are expected while measuring along the main axis and two diagonals. The orientational dependences of the electron-phonon coupling constant, the superconducting energy gaps, and densities of states at the Fermi level [10–14] are expected to affect the shape of $B_c(T)$ curves as well as to change the absolute value of $B_c(0)$. In our experiments, however, all measured $B_c(T)$ dependences were found to coincide within the experimental accuracy. The corresponding deviation functions $D(t)$'s lie just at the top border

*rustem.khasanov@psi.ch

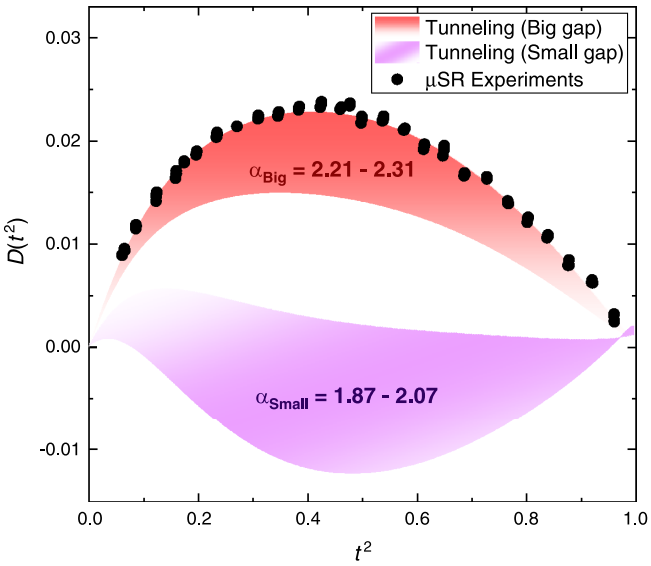

FIG. 1. Deviation of the thermodynamic critical field $B_c(T)$ from the parabolic behavior $[D(t^2) = B_c(t^2)/B_c(0) - (1 - t^2)]$ as expected for the big: $\alpha_{big} = \Delta_{big}/k_B T_c = 2.21$–$2.31$ (red segment) and the small: $\alpha_{small} = \Delta_{small}/k_B T_c = 1.87$–$2.07$ (violet segment) reduced gaps for elemental Pb reported in Refs. [10–12] ($t = T/T_c$ is the reduced temperature). Calculations of $D(t)$ functions are performed by using the α model [23,24]. Black points are the experimental $D(t)$ data measured with the external field B_{ex} applied along three different crystallographic directions: [100], [110], and [111] (see the text for details).

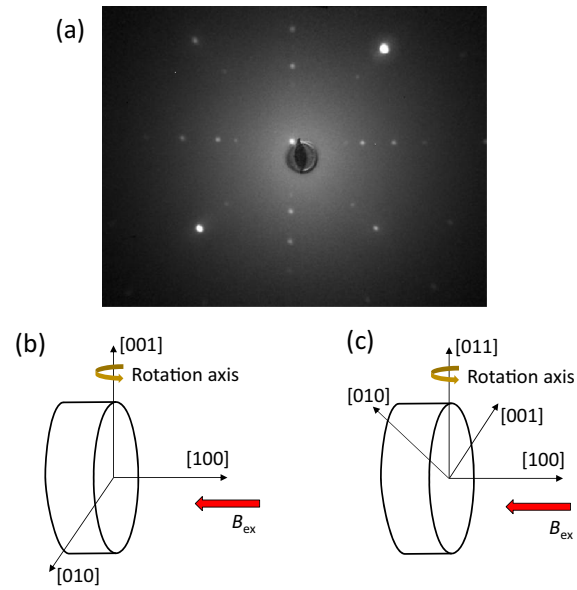

FIG. 2. (a) Laue image of a Pb single crystal. The cubic crystal structure of Pb is clearly visible. (b) The schematic of the first set of experiments (expt. No. 1) allowing sample rotation along the 001 crystal axis. In this configuration $B_{ex} \parallel [100]$ and $B_{ex} \parallel [110]$ sets of measurements were performed. (c) The second set of experiments (expt. No. 2) with the sample rotation along the 011 axis. In these experiments, $B_{ex} \parallel [100]$ and $B_{ex} \parallel [111]$ configurations were probed.

of the big superconducting energy gap branch (see Fig. 1). Our results suggest that elemental Pb is an *isotropic* and a *single-gap* superconductor.

The Pb single-crystal sample was supplied by Goodfellow [25]. The disk-shaped single crystal has the following parameters: orientation—[100], thickness—1.6 mm, diameter—10 mm, and purity—99.999%. Prior to μSR studies, in order to minimize pinning effects, the sample was annealed for 1 week at a temperature of 300 °C, i.e., $\simeq$27 °C below the melting point. The Laue image of the Pb single crystal is presented in Fig. 2(a), which clearly evinces the cubic crystal structure of Pb.

The transverse-field muon-spin rotation/relaxation (TF-μSR) experiments were conducted using the Dolly spectrometer (πE1 beam line) at the Paul Scherrer Institute, Switzerland. Measurements were performed in the intermediate state of superconducting Pb, i.e., when the sample volume is separated into the normal-state and the superconducting-state (Meissner) domains [15,18,22,26–32]. Two sets of experiments were performed. In the first experiment [expt. No. 1, Fig. 2(b)], the sample was rotated along the 001 axis, which allowed for measurements with the external magnetic-field B_{ex} applied parallel to the [100] ($B_{ex} \parallel [100]$) and [110] ($B_{ex} \parallel [110]$) axes. In the second experiment [expt. No. 2, Fig. 2(c)], the sample was rotated along the [011] axis, so the corresponding $B_{ex} \parallel [100]$ and $B_{ex} \parallel [111]$ measurements were performed.

The measurement procedure was as follows. First, a predetermined temperature below the superconducting transition temperature [$T_c(B_{ex} = 0) \simeq 7.2$ K] was stabilized. Second, the sample was turned into the $B_{ex} \parallel [100]$ configuration. Then, B_{ex} was increased up to 85 mT, i.e., above $B_c(0) \simeq$ 80 mT [26,33,34]. Finally, the TF-μSR measurements were performed at fields corresponding to $\simeq$90, 85, 80, and 75% of $B_c(T)$, by considering the $B_c(T)$ curve determined in Refs. [33,34]. By finishing experiments in the $B_{ex} \parallel [100]$ configuration and by keeping the temperature unchanged, the sample was rotated by 45°. After such a rotation, measurements at similar fields were repeated for $B_{ex} \parallel [110]$ [expt. No. 1, Fig. 2(b)] and for $B_{ex} \parallel [111]$ [expt. No. 2, Fig. 2(c)]. Note that the experiments with the sample rotation at constant T, compared to a T scan at a constant angle, ensures that the sample temperature remains the same for two different field orientations. In this case, possible differences in the measured values of the thermodynamic critical fields are caused by intrinsic orientational effects and not by the possible temperature differences/instabilities. This also implies that measurements in the $B_{ex} \parallel [100]$ configuration were performed twice: once in expt. No. 1 and a second time in expt. No. 2.

The magnetic-field distribution in a type-I superconductor in the intermediate state, which is probed directly by means of TF-μSR, consists of two sharp peaks corresponding to the response of the domains remaining in the Meissner state ($B = 0$) and in the normal-state ($B \equiv B_c > B_{ex}$). Consequently, the value of B_c could be directly and very precisely determined by measuring the position of the $B > B_{ex}$ peak [18,22,26–32,35–40]. The details of the TF-μSR experiments on elemental Pb and the data analysis procedure are discussed in the Supplemental Material [41].

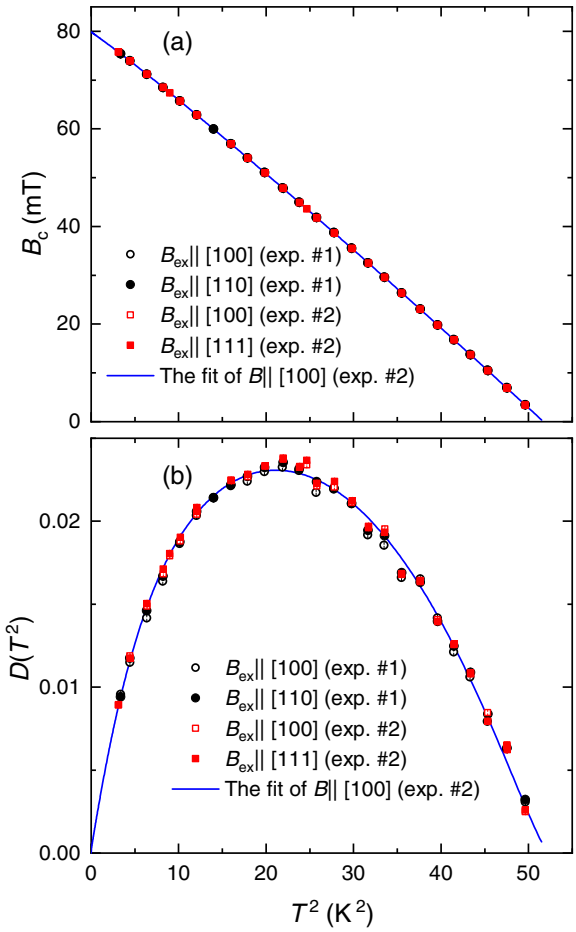

FIG. 3. (a) Temperature dependences of the thermodynamic critical-field B_c of elemental Pb single crystal measured along different crystallographic directions. The solid line is the fit of $B_c(T^2)$ measured in expt. No. 2 in the $B_{ex} \parallel [100]$ configuration by means of Eq. (5). (b) Deviation functions $D(T^2)$ obtained by subtracting parabolic functions from measured $B_c(T^2)$ curves, see Eq. (2). The solid line is the same as in panel (a), but after subtracting the parabolic function.

The results of TF-μSR experiments are summarized in Fig. 3. Panels (a) and (b) represent the temperature evolution of the thermodynamic critical-field B_c and the deviation function D, respectively. Note that within each set of data [$B_c(T^2)$ or $D(T^2)$], the experimental dependences measured along three different crystallographic directions ([100], [110], and [111]) cannot be distinguished from each other. The individual $B_c(T^2)$ and $D(T^2)$ curves are presented in the Supplemental Material [41].

Bearing in mind that in elemental Pb two superconducting energy gaps might be present (see Refs. [10–14] and Fig. 1), the measured $B_c(T)$ dependences should be analyzed within the multigap scenario. Such an approach was recently used by us to describe the two-gap superconductivity in noncentrosymmetric binary alloy AuBe [18,19]. However, as will be shown later, in elemental Pb, the single-gap approach was found to describe the experimental data reasonably precisely, so any type of admixture of the second superconducting energy gap was not expected [see also the single-gap theory curves in panels (a) and (b) of Fig. 3].

The $B_c(T^2)$ curves were analyzed within the framework of the empirical α model [23,24]. Here, the version for strong-coupled superconductors, such as elemental Pb, was employed [23]. It accounts for the fact that in metals with strong electron-phonon coupling, the electronic specific-heat coefficient γ_e is significantly temperature dependent. Consequently, the basic assumptions of the weak-coupled α model,

$$C_{en}(T) = S_{en}(T) = \gamma_e T \tag{3}$$

must be substituted with [42,43]

$$C_{en}(T) = T\frac{\partial S_{en}(T)}{\partial T} = \gamma_0\left[1 + \lambda_{el\text{-}ph}\frac{\gamma_1(T)}{\gamma_1(0)}\right]T. \tag{4}$$

Here, C_{en} and S_{en} are the normal-state electronic specific heat and the electronic entropy, respectively; $\lambda_{el\text{-}ph}$ is the electron-phonon coupling constant; $\gamma_1(T)$ is the function accounting for nonlinear temperature dependence of the electronic specific heat; and γ_0 is the electronic specific-heat coefficient in the absence of electron-phonon coupling. Note that by setting $\lambda_{el\text{-}ph} = 0$, i.e., by ignoring the electron-phonon interaction, Eq. (4) reduces to Eq. (3). For elemental Pb, the quantity $\gamma_1(T)/\gamma_1(0)$ was calculated by Grimvall [42], and it is presented in Fig. S6 in the Supplemental Material [41].

Within the strong-coupling approach, the thermodynamic critical field is further obtained as [23,24]

$$\frac{B_c^2(t)}{8\pi S_{en}(1)} = \int_t^1 \frac{S_{en}(t')}{S_{en}(1)}dt' - \int_t^1 \frac{S_{es}(t')}{S_{es}(1)}dt', \tag{5}$$

with the temperature dependences of the normal-state $S_{en}(t)$ and the superconducting-state $S_{es}(t)$ entropies described as [23,24]

$$S_{en}(t) = \gamma_0 \int_0^t \left[1 + \lambda_{el\text{-}ph}\frac{\gamma_1(t')}{\gamma_1(0)}\right]dt',$$

and

$$S_{es}(t) = \frac{6\alpha^2 S_{en}(1)}{\pi^2 t}\int_0^\infty f(\alpha, E, t)\left(E + \frac{\varepsilon^2}{E}\right)d\varepsilon.$$

Here, $t = T/T_c$ is the reduced temperature, $\alpha = \Delta/k_B T_c$, $f(\alpha, E, t) = [\exp(\alpha E/t) + 1]^{-1}$ is the Fermi function, and $E = E[\varepsilon, \Delta(t)] = \sqrt{\varepsilon^2 + \Delta(t)^2}$ is the quasiparticle energy. The temperature dependence of the normalized gap, tabulated by Mühlschlegel [44] was parametrized as $\Delta(t)/\Delta = \tanh\{1.82[1.018(1/t - 1)]^{0.51}\}$ [19].

The parameters obtained from the analysis of the measured $B_c(T)$ dependences by means of Eq. (5) are summarized in Table I. $\lambda_{el\text{-}ph} = 1.5$ was used, in accordance with $\lambda_{el\text{-}ph} =$ 1.48–1.55 of elemental Pb reported in the literature [4,45–47]. The solid lines in Figs. 3(a) and 3(b) are the fit of Eq. (5) to the $B_c(T)$ obtained in expt. No. 2 with $B_{ex} \parallel [100]$ (fit curves strongly overlap with each other, so only a single curve is shown as a representative manner). The fitting curves for each individual experiment are presented in the Supplemental Material [41].

From the results presented in Fig. 3 and Table I, the following three important points emerge:

TABLE I. The parameters obtained from the analysis of measured $B_c(T)$ dependences in the Pb single crystal within the framework of a strong-coupling α model [23,24]. The meaning of the parameters is the following: T_c is the superconducting transition temperature, $B_c(0)$ is the zero-temperature value of the upper critical field, $\alpha = \Delta/k_B T_c$ is the reduced gap, and Δ is the zero-temperature value of the superconducting energy gap.

Orientation	T_c (K)	$B_c(0)$ (mT)	$\alpha = \frac{\Delta}{k_B T_c}$	Δ (meV)
$B_{ex} \parallel [100]$ (expt. No. 1)	7.193(2)	79.828(4)	2.309(2)	1.431(2)
$B_{ex} \parallel [110]$ (expt. No.1)	7.191(2)	79.852(4)	2.311(2)	1.432(2)
$B_{ex} \parallel [100]$ (expt. No. 2)	7.190(2)	79.847(4)	2.312(2)	1.432(2)
$B_{ex} \parallel [111]$ (expt. No. 2)	7.190(2)	79.871(4)	2.315(2)	1.434(2)
Averaged	7.191(2)	79.850(4)	2.312(2)	1.432(2)

(i) The values of the transition temperature $T_c = 7.191(2)$ K and the thermodynamic critical-field $B_c(0) = 79.850(4)$ mT stay in agreement with the values reported in literature for high quality Pb single-crystal samples [33,34,48]. The tiny $\simeq$2-mK T_c change between the expt. No. 1 and expt. No. 2 could be caused by slightly different thermal contact between the sample and the cryostat's cold plate. Note that the change from expt. No. 1 to expt. No. 2 required regluing of the sample to the cold plate. The same reason explains the 0.019(6) mT difference in $B_c(0)$ values obtained in expt. No. 1 and expt. No. 2 with $B_{ex} \parallel [100]$.

(ii) Experiments with the external magnetic field applied along the diagonal directions ([110] and [111]) show a slight increase in $B_c(0)$ values as compared to the $B_{ex} \parallel [100]$ set of experiments. The corresponding difference is 0.024(6) mT for both diagonal orientations. Bearing in mind that $B_c(0)$ is a measure of the condensation energy [see Eq. (1)] and considering that the superconducting energy gap remains the same within experimental accuracy (see Table I), this would imply that the density of states at the Fermi levels depends on the crystallographic direction. The effect is, however, very small and accounts for $\sim$0.04–0.1% increase in $N_F(0)$ along the [110] and [111] directions.

(iii) The reduced gap, i.e., the ratio of the superconducting energy gap to T_c, does not depend on orientation. For all four measurements performed in three different field orientations (along [100], [110], and [111] crystal axes) the values of $\alpha = \Delta/k_B T_c$ stay the same within experimental uncertainty.

The experimental data obtained in the present Letter are not consistent with the presence of two distinct superconducting energy gaps in elemental Pb for the two following reasons:

First of all, anisotropies of the Fermi-surface sheets formed by two energy bands in elemental Pb are very much different. The so-called "inner" Fermi surface is almost spherical in shape, whereas the "outer" one has a tubular structure [12,13,49]. For this reason, energy gaps associated with each Fermi surface are expected to have different contributions to the thermodynamic quantities, including B_c in various crystallographic directions. Following discussions of Ref. [12], the contribution of the gap opened in the outer (tubular) Fermi surface needs to be highest along [110], intermediate along [100], and smallest along the [111] crystal axes. Considering the fact that gaps opened in the inner and outer Fermi surfaces are different, this would imply the dependence of $B_c(T)$ and so $D(T)$ on the crystallographic direction. Our experiments reveal, however, that all measured $B_c(T)$ and $D(T)$ dependences are identical.

Second, within the two-gap scenario, the deviation curve $D(t^2)$ consists of the contribution from both energy gaps [19]. The presence of two superconducting energy gaps in elemental Pb should let $D(t^2)$ stay somewhere in between or even within the α_{small} and/or α_{big} branches. The experimental $D(t^2)$ points lie, however, on the top of the α_{big} branch (see Fig. 1). Consequently, any admixture of the smaller gap to the measured $D(t^2)$ becomes impossible.

It is worth emphasizing that the results of bulk μSR measurement presented here may not rule out the possibility that the superconducting response of elemental Pb changes by approaching the surface. Following predictions of the self-consistent two-gap model [50–53], even though the superconducting gaps are opened at two different Fermi surfaces, the temperature evolutions, as well as the absolute values of these gaps would stay the same in a case of strongly coupled electronic bands: $\Delta_1(T) = \Delta_2(T) = \Delta(T)$, $T_{c1} = T_{c2} = T_c$. Here indices 1 and 2 denote the first and the second bands, respectively. By decreasing the interband coupling, the gaps start to behave differently, but they are still opened at the same transition temperature: $\Delta_1(T) \neq \Delta_2(T)$, $T_{c1} = T_{c2} = T_c$. Finally, in a case of zero coupling between the bands, the temperature dependencies of the gaps are different, and the gaps vanish at two different temperatures: $\Delta_1(T) \neq \Delta_2(T)$, $T_{c1} \neq T_{c2}$.

Based on the above presented arguments, one may assume that the difference between our μSR measurements where muons stopped at a distance of $\simeq$0.2 mm from the Pb sample surface (see the Supplemental Material [41]) and tunneling experiments, which are sensitive to the top most atomic layer of the material, could be caused by the corresponding decrease in the interband coupling constant. The weakening of the coupling constant between two electronic bands by approaching the surface, would naturally explain the two-gap observation by means of tunneling. An interesting follow up study to consider, would be to perform low-energy muon experiments, which may allow probing down to $\sim$10-nm-thick surface layer [54].

To conclude, measurements of the temperature evolution of the thermodynamic critical-field B_c along three crystallographic directions in elemental Pb were performed by means of muon-spin rotation/relaxation. Experiments which were carried out by applying the external magnetic field along the [100], [110], and [111] crystal axes suggest the presence of a *single* superconducting energy gap with the absolute value *independent* of the crystallographic orientation. Overall, our experiments imply that elemental Pb is an isotropic single-gap superconductor.

The experiments shown in the present Letter were performed at the Swiss Muon Source (SμS), Paul Scherrer Institute (PSI, Switzerland). The research work of R.G. was supported by the Swiss National Science Foundation SNF Grant No. 200021-175935).

[1] H. Kamerlingh Onnes, Commun. Phys. Lab. Univ. Leiden **122 b** (1911); Proc. K. Ned. Akad. Wet. **14**, 113 (1911).

[2] H. Kamerlingh Onnes, Commun. Phys. Lab. Univ. Leiden **133d** (1913); Proc. K. Ned. Akad. Wet. **16**, 113 (1913).

[3] C. P. Poole, R. Prozorov, H. A. Farach, and R. J. Creswick, in *Superconductivity*, Third ed., edited by C. P. Poole, R. Prozorov, H. A. Farach *et al.* (Elsevier, London, 2014).

[4] J. P. Carbotte, Rev. Mod. Phys. **62**, 1027 (1990).

[5] A. J. Bennett, Phys. Rev. **140**, A1902 (1965).

[6] P. G. Tomlinson and J. P. Carbotte, Phys. Rev. B **13**, 4738 (1976).

[7] B. J. C. Van Der Hoeven, Jr. and P. H. Keesom, Phys. Rev. **137**, A103 (1965).

[8] A. W. Overhauser and L. L. Daemen, Phys. Rev. Lett. **61**, 1885 (1988).

[9] J. D. Short and J. P. Wolfe, Phys. Rev. Lett. **85**, 5198 (2000).

[10] B. L. Blackford and R. H. March, Phys. Rev. **186**, 397 (1969).

[11] G. I. Lykken, A. L. Geiger, K. S. Dy, and E. N. Mitchell, Phys. Rev. B **4**, 1523 (1971).

[12] M. Ruby, B. W. Heinrich, J. I. Pascual, and K. J. Franke, Phys. Rev. Lett. **114**, 157001 (2015).

[13] A. Floris, A. Sanna, S. Massidda, and E. K. U. Gross, Phys. Rev. B **75**, 054508 (2007).

[14] T. G. Saunderson, J. F. Annett, B. Újfalussy, G. Csire, and M. Gradhand, Phys. Rev. B **101**, 064510 (2020).

[15] M. Tinkham, *Introduction to Superconductivity* (Krieger, Malabar, 1975).

[16] M. Zehetmayer, H. M. Weber, and E. Schachinger, J. Low Temp. Phys. **133**, 407 (2003).

[17] E. J. Nicol and J. P. Carbotte, Phys. Rev. B **71**, 054501 (2005).

[18] R. Khasanov, R. Gupta, D. Das, A. Amon, A. Leithe-Jasper, and E. Svanidze, Phys. Rev. Research **2**, 023142 (2020).

[19] R. Khasanov, R. Gupta, D. Das, A. Leithe-Jasper, and E. Svanidze, Phys. Rev. B **102**, 014514 (2020).

[20] J. R. Clem, Ann. Phys. (NY) **40**, 268 (1966).

[21] J. R. Clem, Phys. Rev. **153**, 449 (1967).

[22] R. Khasanov and I. I. Mazin, Phys. Rev. B **103**, L060502 (2021).

[23] H. Padamsee, J. E. Neighbor, and C. A. Shiffman, J. Low Temp. Phys. **12**, 387 (1973).

[24] D. C. Johnston, Supercond. Sci. Technol. **26**, 115011 (2013).

[25] Goodfellow, http://www.goodfellow.com/A/Lead-Single-Crystal.html

[26] C. Kittel, *Introduction to Solid State Physics*, 7th ed. (Wiley, New York, 2007).

[27] P. G. de Gennes, *Superconductivity of Metals and Alloys* (Benjamin, New York, 1966).

[28] R. Prozorov, Phys. Rev. Lett. **98**, 257001 (2007).

[29] R. Prozorov, A. F. Fidler, J. R. Hoberg, and P. C. Canfield, Nat. Phys. **4**, 327 (2008).

[30] R. Khasanov, M. M. Radonjić, H. Luetkens, E. Morenzoni, G. Simutis, S. Schönecker, W. H. Appelt, A. Östlin, L. Chioncel, and A. Amato, Phys. Rev. B **99**, 174506 (2019).

[31] R. Karl, F. Burri, A. Amato, M. Donegà, S. Gvasaliya, H. Luetkens, E. Morenzoni, and R. Khasanov, Phys. Rev. B **99**, 184515 (2019).

[32] R. Khasanov, H. Luetkens, A. Amato, and E. Morenzoni, Phys. Rev. B **101**, 054504 (2020).

[33] G. Chanin and J. P. Torre, Phys. Rev. B **5**, 4357 (1972).

[34] N. B. Brandt, I. V. Berman, and Y. P. Kurkin, Zh. Eksp. Teor. Fiz. **69**, 1710 (1975).

[35] V. S. Egorov, G. Solt, C. Baines, D. Herlach, and U. Zimmermann, Phys. Rev. B **64**, 024524 (2001).

[36] M. Gladisch, D. Herlach, H. Metz, H. Orth, G. zu Putlitz, A. Seeger, H. Teichler, W. Wahl, and W. Wigand, Hyperfine Interact. **6**, 109 (1979).

[37] V. G. Grebinnik, I. I. Gurevich, V. A. Zhukov, A. I. Klimov, L. A. Levina, V. N. Maiorov, A. P. Manych, E. V. Mel'nikov, B. A. Nikol'skii, A. V. Pirogov, A. N. Ponomarev, V. S. Roganov, V. I. Selivanov, and V. A. Suetin, Zh. Eksp. Teor. Fiz. **79**, 518 (1980).

[38] H. Leng, J.-C. Orain, A. Amato, Y. K. Huang, and A. de Visser, Phys. Rev. B **100**, 224501 (2019).

[39] J. Beare, M. Nugent, M. N. Wilson, Y. Cai, T. J. S. Munsie, A. Amon, A. Leithe-Jasper, Z. Gong, S. L. Guo, Z. Guguchia, Y. Grin, Y. J. Uemura, E. Svanidze, and G. M. Luke, Phys. Rev. B **99**, 134510 (2019).

[40] V. Kozhevnikov, A. Suter, T. Prokscha, and C. Van Haesendonck, J. Supercond. Novel Magn. **33**, 3361 (2020).

[41] See Supplemental Material at https://link.aps.org/supplemental/10.1103/PhysRevB.104.L100508 for a description of the data analysis procedure and individual presentation of the analyzed data, which includes Refs. [55–61].

[42] G. Grimvall, Phys. Kondens. Mater. **9**, 283 (1969).

[43] F. Giustino, Rev. Mod. Phys. **89**, 015003 (2017).

[44] B. Mühlschlegel, Z. Phys. **155**, 313 (1959).

[45] R. C. Dynes, Solid State Commun. **10**, 615 (1972).

[46] R. C. Dynes and J. M. Rowell, Phys. Rev. B **11**, 1884 (1975).

[47] P. B. Allen, Phys. Rev. B **36**, 2920(R) (1987).

[48] B. T. Matthias, T. H. Geballe, and V. B. Compton, Rev. Mod. Phys. **35**, 1 (1963).

[49] J. R. Anderson and A. V. Gold, Phys. Rev. **139**, A1459 (1965).

[50] H. Suhl, B. T. Matthias, and L. R. Walker, Phys. Rev. Lett. **3**, 552 (1959).

[51] A. Bussmann-Holder, R. Micnas, and A. R. Bishop, Eur. Phys. J. B **37**, 345 (2004).

[52] V. G. Kogan, C. Martin, and R. Prozorov, Phys. Rev. B **80**, 014507 (2009).

[53] R. Gupta, C. Löhnert, C. Wang, D. Johrendt, H. Luetkens, S. Malick, T. Shiroka, Z. Hossain, and R. Khasanov, Phys. Rev. B **102**, 144515 (2020).

[54] E. Morenzoni, T. Prokscha, A. Suter, H. Luetkens, and R. Khasanov, J. Phys.: Condens. Matter **16**, S4583 (2004).

[55] http://www.cmr-direct.com/en/ge-varnish.

[56] http://www.srim.org/.

[57] A. Amato, H. Luetkens, K. Sedlak, A. Stoykov, R. Scheuermann, M. Elender, A. Raselli, and D. Graf, Rev. Sci. Instrum. **88**, 093301 (2017).

[58] https://apiezon.com/products/vacuum-greases/apiezon-n-grease/.

[59] R. Khasanov, Z. Guguchia, I. Eremin, H. Luetkens, A. Amato, P. K. Biswas, C. Rüegg, M. A. Susner, A. S. Sefat, N. D. Zhigadlo, and E. Morenzoni, Sci. Rep. **5**, 13788 (2015).

[60] A. Yaouanc, and P. Dalmas de Réotier, *Muon Spin Rotation, Relaxation and Resonance: Applications to Condensed Matter* (Oxford University Press, Oxford, 2011).

[61] P. B. Allen and M. L. Cohen, Phys. Rev. B **1**, 1329 (1970).